NON-DARCIAN SURFACE TENSION EFFECTS ON FREE SURFACE TRANSPORT IN POROUS MEDIA

S. C. Chen and K. Vafai
Department of Mechanical Engineering, Ohio State University, Columbus, Ohio 43210, USA

The phenomenological analysis of free surface transport through porous media using the Brinkman–Forchheimer–extended Darcy model is presented. A finite difference scheme using the marker-and-cell (MAC) method is employed to investigate the momentum and energy transport in a porous channel involving free surface transport phenomena. The interfacial tension effect at the free surface is incorporated in the analysis. The present investigation constitutes one of the first numerical investigations of the free surface momentum and energy transport through porous media using the MAC method. Fully developed velocity and temperature fields for saturated as well as unsaturated porous channels, for cases with different Darcy numbers, are compared and verified against existing analytical solutions. Temporal free surface distributions for cases with different Darcy numbers and Reynolds numbers are presented. Also explored is the effect of the free surface transport in porous media on the energy transfer. It is found that the boundary and inertial effects have a significant influence on the free surface transport through porous media and that the surface tension effects become insignificant for $Re_K > 1$. The present work constitutes one of the first studies on Non-Darcian effects on free surface transport in porous media.

INTRODUCTION

The prediction of the fluid interface displacement has become increasingly important in some manufacturing processes, such as resin transfer molding (RTM), structure reaction injection molding (SRIM), gas-assisted injection molding, die filling processes, and clean-up of refineries. Related studies have also been performed in the oil industry to understand the simultaneous flow of oil, water, and gas in porous strata during the production of oil from oil fields. The study of linear encroachment was done by Muskat [1], where a one-dimensional Darcy's flow model was used to investigate two fluids moving in a narrow channel. A comprehensive analytical study was done by Srinivasan and Vafai [2] to obtain a further understanding and better prediction of the interface for the linear encroachment in an immiscible two-fluid system in which the boundary and inertial effects were accounted for in the study of linear encroachment. The work by Chen and Vafai [3] describes one of the first applications of the marker-and-cell (MAC) method for investigating the free surface momentum and energy transport in porous media.

Received 5 July 1996; accepted 10 September 1996.
Address correspondence to Professor Kambiz Vafai, Department of Mechanical Engineering, Ohio State University, 206 W. 18th Avenue, Columbus, OH 43210-1107, USA.

Numerical Heat Transfer, Part A, 31:235–254, 1997

1040–7782/97 $12.00 + .00

NOMENCLATURE

Da	Darcy number $[= K/(H^2\theta)]$	u_D	Darcian convective velocity $[= -K/\mu_f(dp/dx)]$
h	heat transfer coefficient	U	velocity vector
H	half of the channel height	x_i	initial location of the fluid
k_e	effective thermal conductivity of the porous matrix	x_0	free surface location
K	permeability, m^2	α_m	effective thermal diffusivity
L	horizontal extent of the channel	Δp	pressure difference across the encroaching fluid, N/m^2
n_x	local normal vector to free surface in x direction	ε	mobility ratio (μ_2/μ_1)
n_y	local normal vector to free surface in y direction	θ	porosity of the porous medium
p	pressure	κ_ξ	sum of curvature at the free surface
p_e	entrance pressure	μ_f	fluid viscosity
P_ξ	capillary pressure at the free surface	μ_1	residing fluid viscosity
p_∞	ambient pressure	μ_2	encroaching fluid viscosity
Re_K	Reynolds number $(= u_D\sqrt{K}/\nu_f)$	ν_f	kinematic viscosity
T_e	entrance temperature	ρ_f	fluid density
T_m	mean temperature $[= (\int_0^H uT\,dy)/(u_D H)]$	σ	surface tension coefficient, N/m

It should be noted that, for example, for the RTM/SRIM process, an appropriate simulation for the filling process is necessary to facilitate the design of a mold. A few studies have been performed by Young et al. [4] and Bruschke and Advani [5] using the control volume finite element method. In their investigations, simple boundary conditions at the moving front were employed, and surface tension effect was not included. For RTM, using simple free surface boundary conditions and neglecting surface tension forces can be reasonable assumptions. Furthermore, since the permeability is very low, the use of the Darcy model may be appropriate. However, for SRIM, the pressure and velocity fields are much higher, which can result in significant non-Darcian effects. Inappropriate prediction of the temperature field at the free surface could result in inaccurate distribution of reaction rate. This, in turn, affects the viscosity of the resin, since most conversion occurs at the interface, and the resin viscosity heavily depends on the conversion rate [6]. Therefore, to predict the interface conditions accurately, a more comprehensive set of boundary conditions associated with free surface transport and non-Darcian effects must be considered.

The present work aims at an investigation of free surface transport while incorporating boundary and inertia effects. One fluid initially saturates the porous channel, and the pressure field at the free surface is assumed to be fixed. The analysis developed here is built on that utilized by Vafai and Chen [7] and Chen and Vafai [3]. The numerical investigation used here is based on the MAC method, which was originally developed at the Los Alamos Laboratory by Harlow and Welch [8]. This method utilizes the primitive variables, namely, pressure and velocity components, in a staggered grid system while incorporating the Eulerian fluid cells and the coordinates of a set of marker particles to track the free surface

position. Several applications were studied in detail, based on the early version of the MAC method. To this end, a technique including surface stress condition and curvature effects was introduced by Daly and Pracht [9], while Hirt and Shannon [10], in their study of a viscous core, investigated the limits of the original version of the MAC method. They demonstrated that with a simple modification, it is possible to approximate the complete normal stress condition, and this modification was shown to have a pronounced effect on some low Reynolds number flows. Furthermore, modifications on the details of the numerical method, such as interpolation schemes and more exact application of the pressure boundary condition, were made by Chan and Street [11] in their numerical study of finite amplitude water waves. Hirt et al. [12] incorporated the complete free surface stress conditions into a numerical technique in their study of viscous bore. Frederiksen and Watts [13], using an iterative finite element technique, studied entrainment of fluid by a vertically moving plate from a bath of fluid of finite depth and the consequent formation of a thin film of fluid on the plate. More recently, an experimental investigation of free surface transport and subsequent bifurcation and adhesion for a hollow glass ampule was done by Chen and Vafai [14].

In the present study, the normal force introduced by the surface tension effect at the free surface is included in the free surface pressure boundary condition. The temporal free surface distributions are presented and compared to the Darcy model [3]. The comparisons of temporal free surface and pressure distributions with and without surface tension effect are shown in this work. In addition, the boundary and inertial effects on free surface transport through porous media are analyzed in some detail.

ANALYSIS

Figure 1 presents a schematic diagram of the present study. In this study a specified fluid 2 initially resides in the porous channel.

Governing Equations

As shown in the work of Vafai and Tien [15], the velocity field develops in very short distance of the order of $Ku_D \nu_f^{-1}$ from the entrance. Therefore the

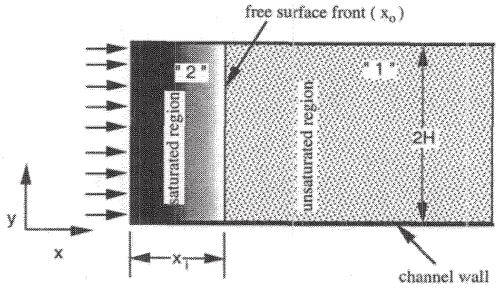

Figure 1. Free surface transport through a porous channel.

convective terms are neglected, as they are only important within a very short distance. In addition, it has been shown in the work of Vafai and Tien [16] that the steady state momentum field is established within a very short time period. Therefore the time dependent terms are also neglected in the momentum equation. Assuming local thermal equilibrium [17], and using the local volume averaging technique, the continuity, momentum, and energy equations are obtained as follows.

Continuity

$$\frac{\partial u}{\partial x} + \frac{\partial v}{\partial y} = 0 \tag{1}$$

Momentum

$$-\frac{\theta}{\rho_f}\bar{\nabla}p_f + \frac{\mu_f}{\rho_f}\nabla^2 U - \left(\frac{\mu_f \theta U}{K\rho_f} + \frac{FU\theta|U|}{\sqrt{K}}\right) = 0 \tag{2}$$

Energy

$$u\frac{\partial T}{\partial x} + v\frac{\partial T}{\partial y} = \alpha_m\left(\frac{\partial^2 T}{\partial^2 x} + \frac{\partial^2 T}{\partial^2 y}\right) \tag{3}$$

In the above equations, p_f represents the pressure read off a pressure gauge, μ_f the fluid viscosity, ρ_f the fluid density, K the permeability of the porous medium, θ the porosity, F the inertia constant, as defined by Vafai and Tien [16], and α_m the effective thermal diffusivity of the porous channel. The experimental procedure for determining the values of K and F are described by Vafai and Tien [16]. The typical values of K and the given functional dependence of F can be deduced from a number of empirical results such as those of Koh et al. [18]. In the present study, both x and y momentum equations are solved [19].

The boundary, initial, and interface conditions required to solve the governing equations are expressed as follows.

Boundary conditions

$$p = p_e \qquad v = 0 \qquad T = T_e \qquad x = 0 \tag{4}$$

$$\frac{\partial u}{\partial x} = 0 \qquad -k_e\frac{\partial T}{\partial n} = h(T - T_\infty) \qquad x = x_0 \tag{5}$$

$$u = v = 0 \qquad T = T_w \qquad y = 0 \qquad y = 2H \tag{6}$$

$$p_\xi = \sigma_{eff}\kappa_\xi + 2\mu\left[n_x^2\frac{\partial u}{\partial x} + n_x n_y\left(\frac{\partial u}{\partial y} + \frac{\partial v}{\partial x}\right) + n_y^2\frac{\partial v}{\partial y}\right] \qquad x = x_0 \tag{7}$$

Initial condition

$$u = v = 0 \qquad T = T_\infty \qquad x = x_i \qquad t = 0 \tag{8}$$

where x_0 represents the free surface position, p_e the entrance pressure, P_ξ the capillary pressure at the free surface, σ the surface tension coefficient, κ_ξ the sum of curvature at the free surface, T_e the entrance temperature, T_w the wall temperature, T_∞ the ambient temperature, x_i the initial position of the free surface, h the heat transfer coefficient, k_e the effective thermal conductivity.

Equation (7) presents the complete formulation for the pressure field at the free surface, including the surface tension and viscous effects. The surface tension effect introduced in this work is used to account for the curvature variation when the no-slip boundary condition is imposed. This is the first time surface tension effect is accounted for in a porous channel involving free surface transport. Based on the work by Vafai and Chen [7], the pressure caused by the viscous force will be insignificant. Therefore, Eq. (7) reduces to

$$p_\xi = \sigma_{\text{eff}} \kappa_\xi \tag{9}$$

The general form of the initial condition for the free surface location is based on practical applications such as in injection molding. It is based on some fluid residing in the porous channel where a high pressure is applied at the entrance of the channel.

Numerical Methodology

The finite difference formulation for the governing equations is based on the work by Vafai and Chen [7]. A brief description of the discretization of the governing equation is presented as follows.

x Momentum

$$\left[-\frac{\theta}{\rho_f} \frac{\partial p_f}{\partial x} + \frac{\mu_f}{\rho_f} \nabla^2 u - \left(\frac{\mu_f \theta u}{K \rho_f} + \frac{Fu\theta|U|}{\sqrt{K}} \right) \right] = 0 \tag{10}$$

y Momentum

$$\left[-\frac{\theta}{\rho_f} \frac{\partial p_f}{\partial y} + \frac{\mu_f}{\rho_f} \nabla^2 v - \left(\frac{\mu_f \theta v}{K \rho_f} + \frac{Fv\theta|U|}{\sqrt{K}} \right) \right] = 0 \tag{11}$$

Equations (10) and (11) can be written as

$$-\frac{\theta}{\rho_f} \frac{\partial p_f}{\partial x} + f(x, y) = 0 \tag{12}$$

$$-\frac{\theta}{\rho_f} \frac{\partial p_f}{\partial y} + g(x, y) = 0 \tag{13}$$

where $f(x, y)$ and $g(x, y)$ are defined as

$$f(x, y) = \frac{\mu_f}{\rho_f}\nabla^2 u - \left(\frac{\mu_f \theta u}{K\rho_f} + \frac{Fu\theta|U|}{\sqrt{K}}\right) \tag{14}$$

$$g(x, y) = \frac{\mu_f}{\rho_f}\nabla^2 v - \left(\frac{\mu_f \theta v}{K\rho_f} + \frac{Fv\theta|U|}{\sqrt{K}}\right) \tag{15}$$

Taking divergence of Eqs. (12) and (13) will result in the following equation:

$$\overline{\nabla}^2 p_f = \frac{\rho_f}{\theta}\left(\frac{\partial f(x, y)}{\partial x} + \frac{\partial g(x, y)}{\partial y}\right) \tag{16}$$

The successive overrelaxation (SOR) method is employed in solving the discretized momentum and pressure equations. As mentioned earlier, the MAC method is utilized to track the temporal free surface position. During the process, extrapolation of the velocity fields in the empty cells is required to carry out the numerical iteration of the momentum and pressure equations. Calculation of the marker particle velocities is accomplished using the obtained velocity field to move the free surface position. An implicit scheme is used to solve the energy equation. The basic aspects of the above-mentioned schemes are presented in the work of Vafai and Chen [7]. The implementation of the present numerical scheme will not be presented here for the sake of brevity.

RESULTS AND DISCUSSION

Comparisons of fully developed velocity and temperature fields, with the exact solution by Vafai and Kim [20], are presented in Figure 2. The fully developed velocity and temperature fields were obtained by solving the governing equations for the configuration shown in Figure 1. As shown in Figure 2*a*, for Da = 1.1×10^{-3}, 1.0×10^{-5}, and 1.0×10^{-6}, the momentum boundary layer thickness is of the order of $(K/\theta)^{1/2}$, which is consistent with the results first given by Vafai and Tien [15]. In order to capture the momentum boundary layer, a variable grid size is employed with a very fine grid structure close to the wall. The difference between the current numerical result and that of the analytical solution given by Vafai and Kim [20] is less than 0.4%. Referring to Figure 2, the numerical results coincide with the analytical results. The same accuracy is obtained for the temperature field as presented in Figure 2*b*. The excellent agreement shown in Figure 2 further confirms the robustness of the employed numerical scheme.

Table 1 illustrates the values of Da (Darcy number), Re_K (Reynolds number), and σ (surface tension coefficient) for all cases studied in the present work. Four cases are studied using the Brinkman–Forchheimer–extended Darcy model. Referring to Table 1, a Darcy number of 1.0×10^{-3} is applied for cases 1, 2, 3, and 4 at Reynolds numbers 1.8×10^{-3}, 1.8×10^{-2}, 1.8×10^{-1}, and 1.8, respectively. The

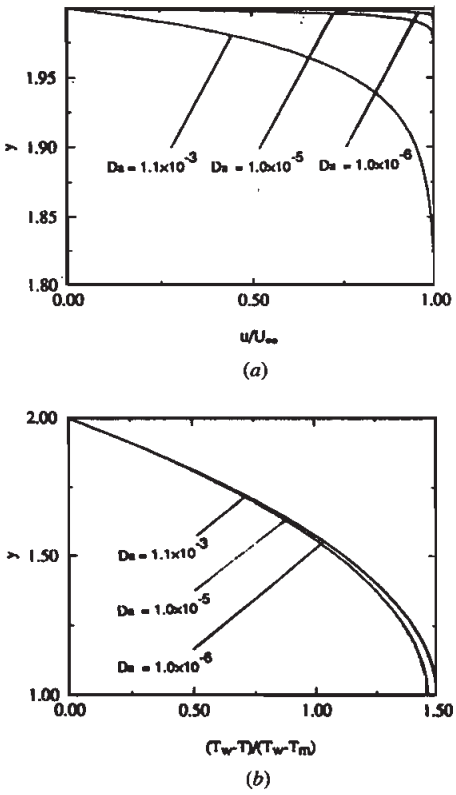

Figure 2. Comparison of fully developed velocity and temperature fields with the analytical solutions by Vafai and Kim [20]: (*a*) velocity field and (*b*) temperature field for Da = 1.1×10^{-3}, 1.0×10^{-5}, and 1.0×10^{-6}.

surface tension effect is not included in cases 1–4, so that impact of the viscous effect on free surface transport can be studied. The surface tension effect is presented separately. A comparison of the temporal free surface distributions at the center of the channel with Darcy's model is presented in Figure 3. Figure 4 illustrates the temporal free surface front distributions at selected time frames for

Table 1. List of input parameters for cases 1–9

Case	Da	Re_K	Capillary effects included
1	1.0×10^{-3}	1.8×10^{-3}	no
2	1.0×10^{-3}	1.8×10^{-2}	no
3	1.0×10^{-3}	1.8×10^{-1}	no
4	1.0×10^{-3}	1.8	no
5	1.0×10^{-3}	1.8×10^{-3}	yes
6	1.0×10^{-3}	1.8×10^{-2}	yes
7	1.0×10^{-3}	1.8×10^{-1}	yes
8	1.0×10^{-3}	0.57	yes
9	1.0×10^{-2}	0.57	yes

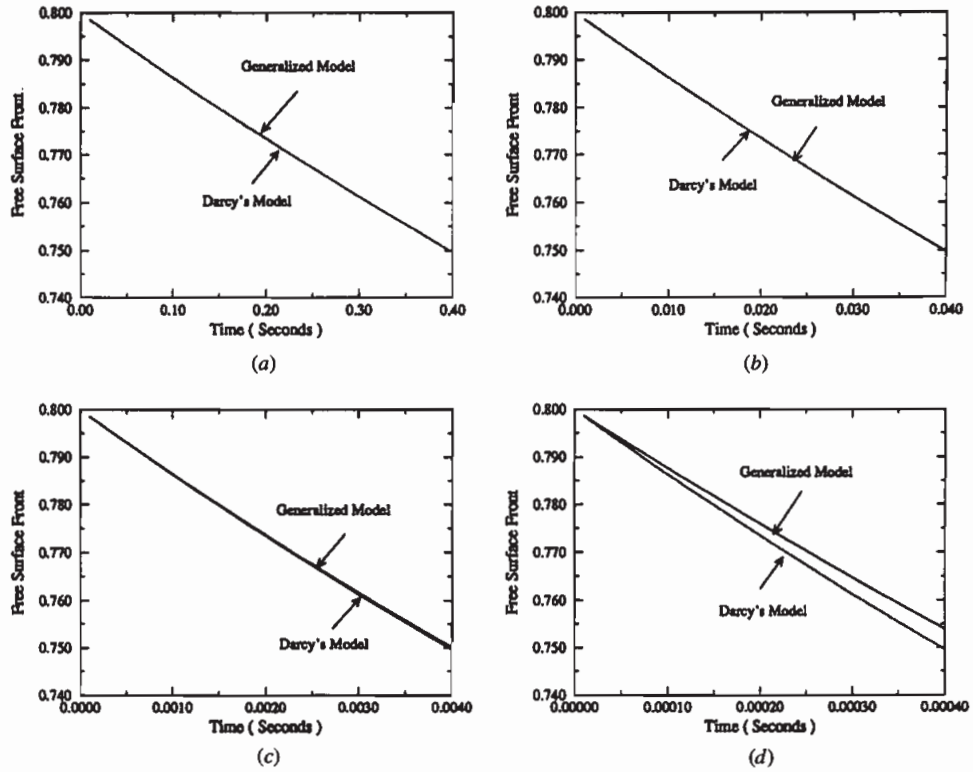

Figure 3. Comparison of temporal free surface positions at the centerline of the channel between generalized (Darcy–Forchheimer–Brinkman) model and Darcy's model without surface tension effect: (*a*) $\mathrm{Re}_K = 1.8 \times 10^{-3}$, (*b*) $\mathrm{Re}_K = 1.8 \times 10^{-2}$, (*c*) $\mathrm{Re}_K = 1.8 \times 10^{-1}$, and (*d*) $\mathrm{Re}_K = 1.8$.

each case. The pressure difference across the saturated portion is assumed to be constant throughout the process, and the encroaching fluid occupies a portion of the channel initially.

As seen in Figure 3, a larger pressure difference results in a shorter time for the encroaching fluid to saturate the same portion of the channel. Furthermore, as depicted in Figure 3, viscous and inertia effects to the free surface motion become more significant as Re_K increases. In Figure 3*a*, with $\mathrm{Re}_K = 1.8 \times 10^{-3}$ for case 1, the difference between Darcy's model and the generalized model is not significant. However, for case 2 ($\mathrm{Re}_K = 1.8 \times 10^{-2}$) the difference starts to increase slightly (Figure 3*b*). As Re_K increases to 1.8×10^{-1} for case 3, the deviation becomes more visible (Figure 3*c*). For case 4 with $\mathrm{Re}_K = 1.8$, the deviation becomes quite significant, as shown in Figure 3*d*. Figure 4 presents comparisons of two-dimensional free surface distributions at selected times for cases 1–4 for the generalized and Darcy's models. Referring to Figure 4*a*, the free surface positions match quite well with Darcy's model except for the area close to the wall. When the no-slip condition is invoked, the point at the wall does not move, resulting in an unsaturated area near the wall. As shown in Figure 4*a*, the distance between the

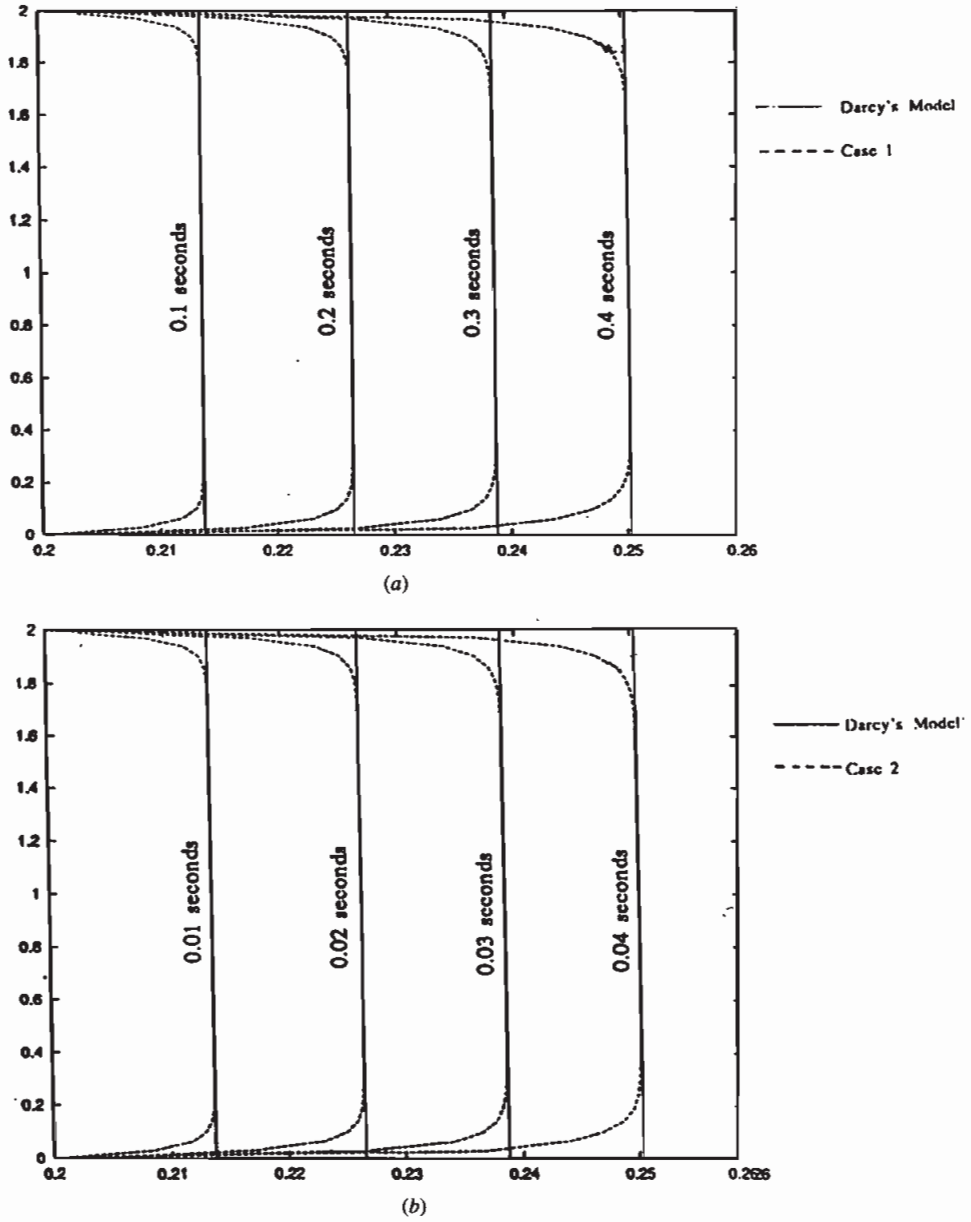

Figure 4. Comparisons of temporal free surface positions of generalized model and Darcy's model without surface tension effect: (*a*) case 1, $\mathrm{Re}_K = 1.8 \times 10^{-3}$; (*b*) case 2, $\mathrm{Re}_K = 1.8 \times 10^{-2}$.

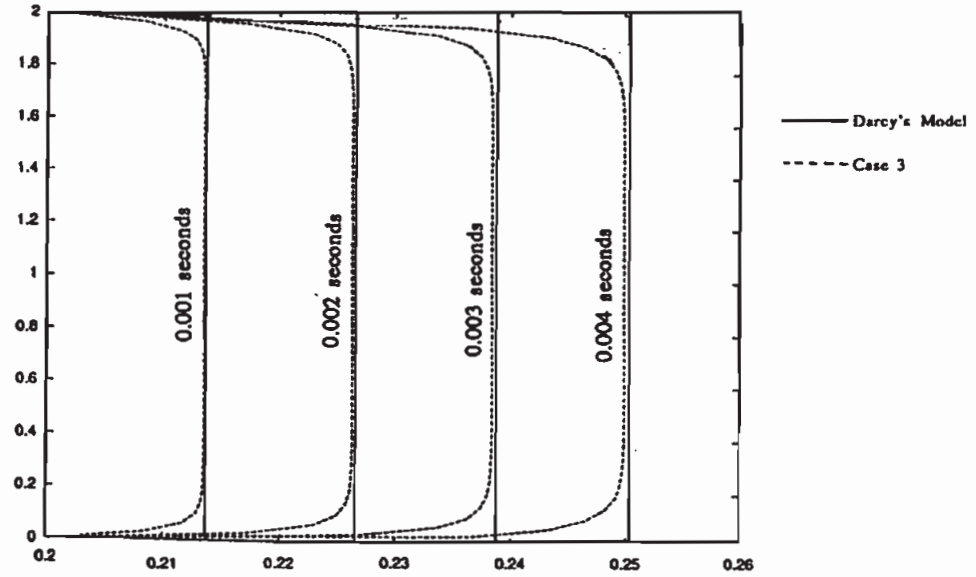

(*c*)

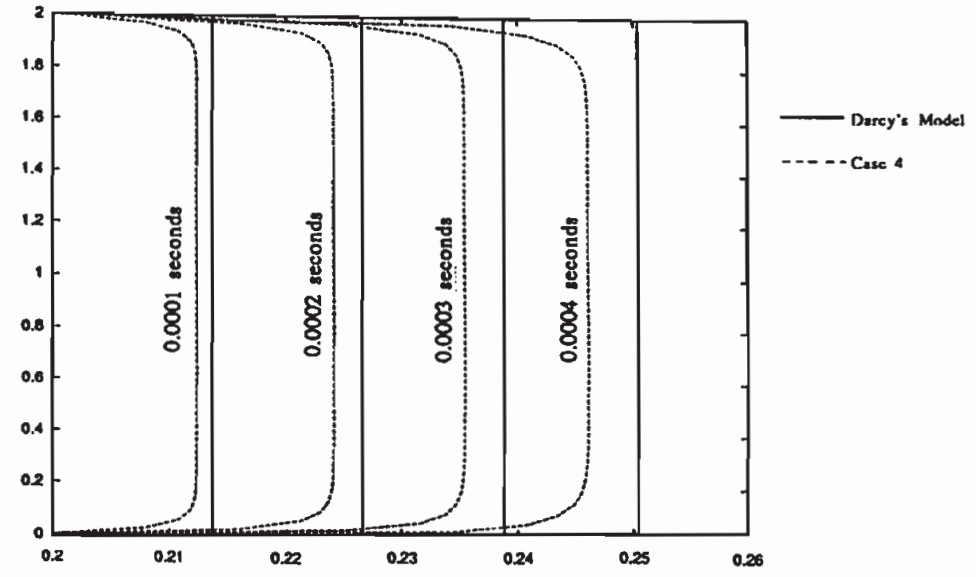

(*d*)

Figure 4. Comparisons of temporal free surface positions of generalized model and Darcy's model without surface tension effect (*Continued*): (*c*) case 3, $\mathrm{Re}_K = 1.8 \times 10^{-1}$; (*d*) case 4, $\mathrm{Re}_K = 1.8$.

saturated zone and the channel wall decreases with time. This is due to the vertical velocity component resulting from the vertical pressure gradient. Figures 5*a* and 5*b* depict the pressure distributions at a time of 0.4 s for case 1. In Figure 5*a*, for Darcy's model, there is only an axial pressure gradient. However, when the no-slip condition is applied, a vertical pressure gradient is formed, as shown in Figure 5*b*. This pressure gradient pushes the fluid toward the wall region, thereby reducing the unsaturated area. As can be seen in Figure 4, it is not until case 3, where the free surface displacement at the centerline region becomes visible for the two models (Figure 4*c*). At the beginning of the process for case 3, the generalized model produces a centerline velocity that is quite close to that obtained by Darcy's model. However, as the process progresses, the difference becomes more significant. For case 4, as shown in Figure 4*d*, for a higher Re_K, the difference in free surface distribution occurs from the beginning of the process.

Figure 6 presents the temperature contours and Nusselt number distributions along the axial direction for case 1. Similar temperature contours and Nusselt number distributions are obtained for cases 2, 3, and 4, and therefore they are presented for brevity. Referring to Figures 6*a* and 6*b*, the temperature distribution

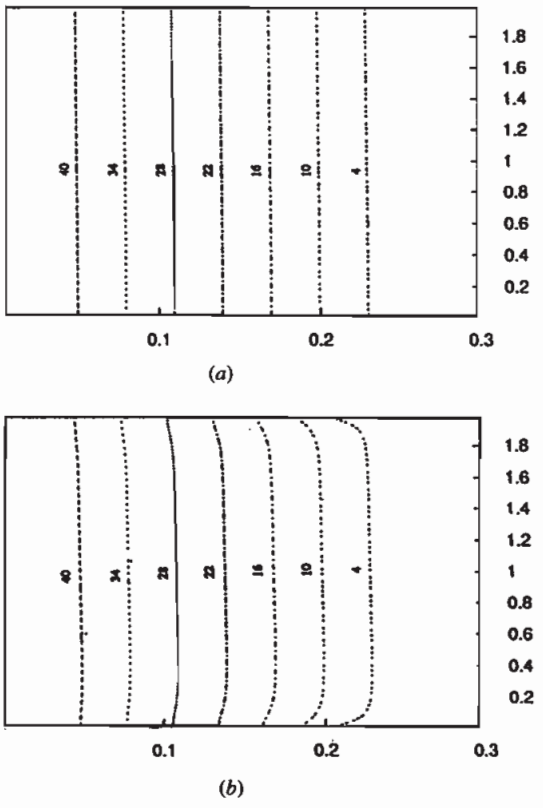

Figure 5. Temporal pressure distributions at 0.4 s for case 1: (*a*) Darcy's model and (*b*) generalized model.

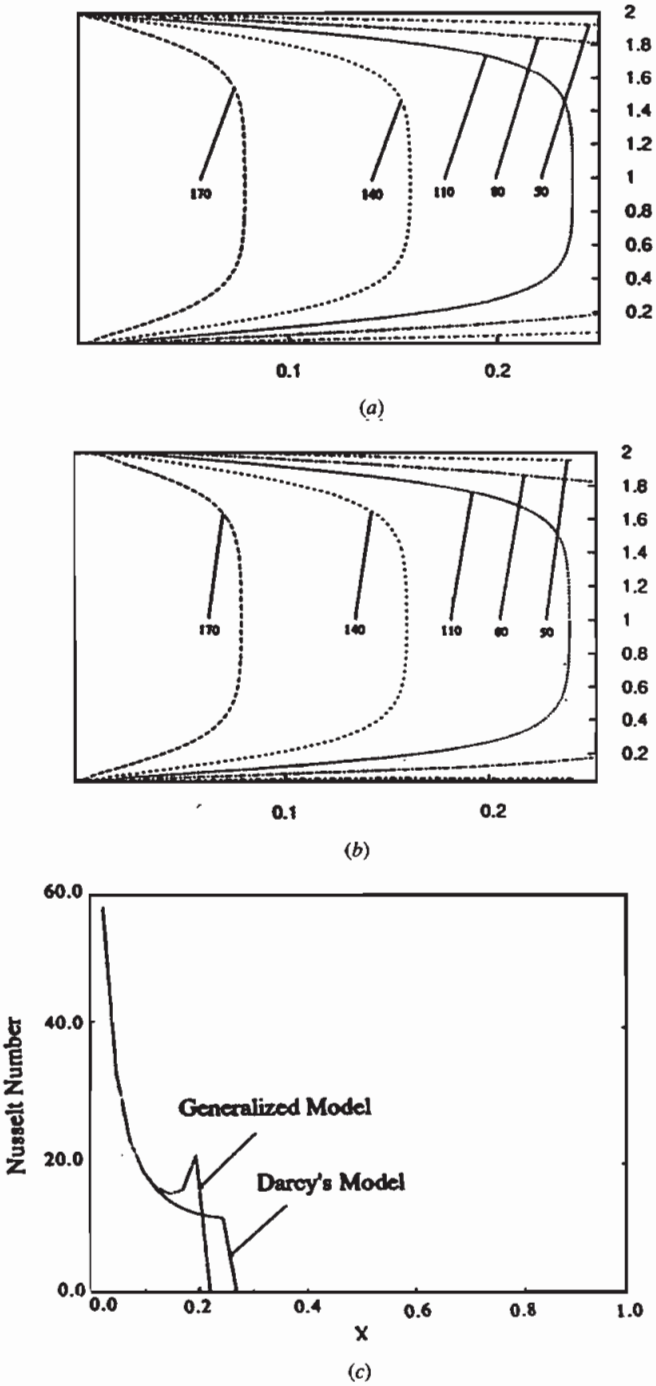

Figure 6. Temporal temperature distributions at 0.4 s for case 1: (*a*) Darcy's model, (*b*) generalized model, and (*c*) axial Nusselt distribution.

near the entrance region for the generalized model is very close to that of Darcy's model. However, the temperature gradient becomes higher near the free surface area for the generalized model. The reason for the higher temperature gradient for the generalized model is the convective boundary condition at the free surface, which is not as efficient as heat conduction through the channel wall. Referring to Figure 6*c*, a higher temperature gradient near the free surface area results in a higher Nusselt number for the generalized model. It should be noted that this situation is different from that of a fully saturated flow through a channel. In this case, the free surface creates an unsaturated region that leads to this behavior.

For Darcy's model, it is appropriate not to account for the surface tension effect because the free surface is always flat, corresponding to zero surface curvature and zero capillary pressure [Eq. (7)]. However, when the no-slip boundary condition is invoked, the free surface is no longer flat, and neglecting the surface tension effect could result in underprediction or overprediction of the free surface motion, depending on the shape of the free surface front. Three cases are investigated to gain an understanding of the surface tension effect on the temporal free surface movement, pressure distribution, and temperature distribution. Referring to Table 1, cases 5, 6, and 7 use the same input parameters as cases 1, 2, and 3, respectively, except that the surface tension effect is accounted for.

Figure 7 shows the comparison of temporal free surface distribution at four time frames for cases 5, 6, and 7. As depicted in Figure 7*a*, the difference between case 5 and case 1 resulting from the surface tension effect is insignificant early on. However, it becomes more significant at later times. This phenomenon can be explained on the basis of the pressure distributions. Early on in the filling process, the free surface configuration is quite flat; thus the capillary pressure distribution along the interface is insignificant in comparison with the applied pressure difference. At a later stage, distortion of the free surface distribution near the wall region becomes prominent, and the free surface motion is affected by the induced capillary pressure at the free surface. For example, for cases 1 and 5, the applied pressure difference is 50 N/m^2, and the resultant capillary pressure for case 5 at 0.4 s is about 5 N/m^2, which is of the same order of magnitude as the applied pressure difference. Without the surface tension effect, the pressure boundary layer thickness (the region over which the pressure distortion occurs) near the free surface is close to the momentum boundary thickness. However, when the surface tension effect is included, the pressure boundary thickness near the free surface decreases owing to the capillary pressure contribution. As can be seen in Figure 7*a*, the unsaturated area for case 5 is larger than case 1. In case 1, the vertical pressure gradient creates a vertical flow field, which reduces the unsaturated area, however, in case 5, distortion of the pressure field creates a flow toward the centerline of the channel (referring to Figure 8*a*). From a practical point of view, pressure distortion is disadvantageous for the filling process because it is blocking the flow toward the channel wall.

Referring to Figure 7*b*, distortion of the flow field becomes less significant for case 6. By examining the pressure distribution shown in Figure 8*b*, it can be seen that the induced capillary pressure is not large enough to create the same type of high-pressure field as in case 5. This is because the capillary pressure is only about 2% of the applied pressure difference. As the Reynolds number is

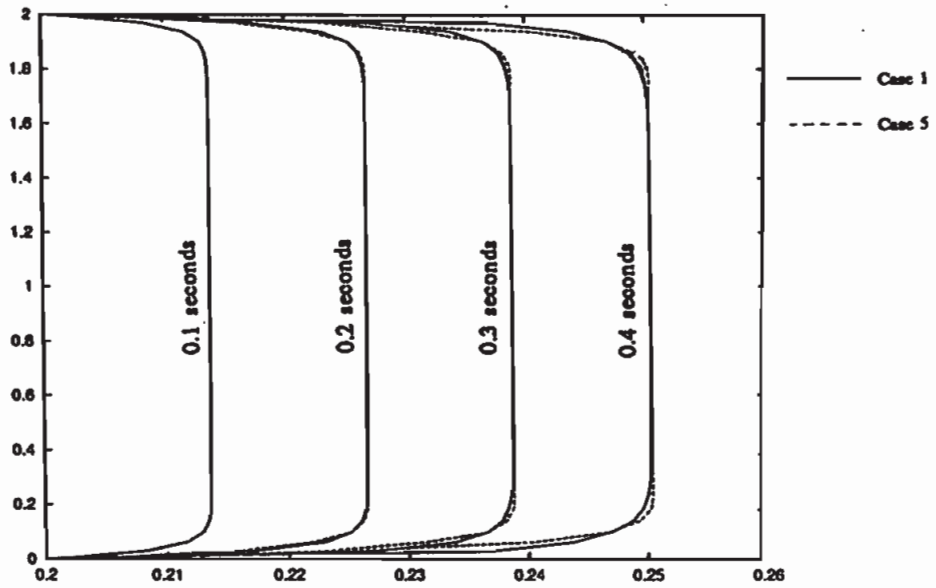

(*a*)

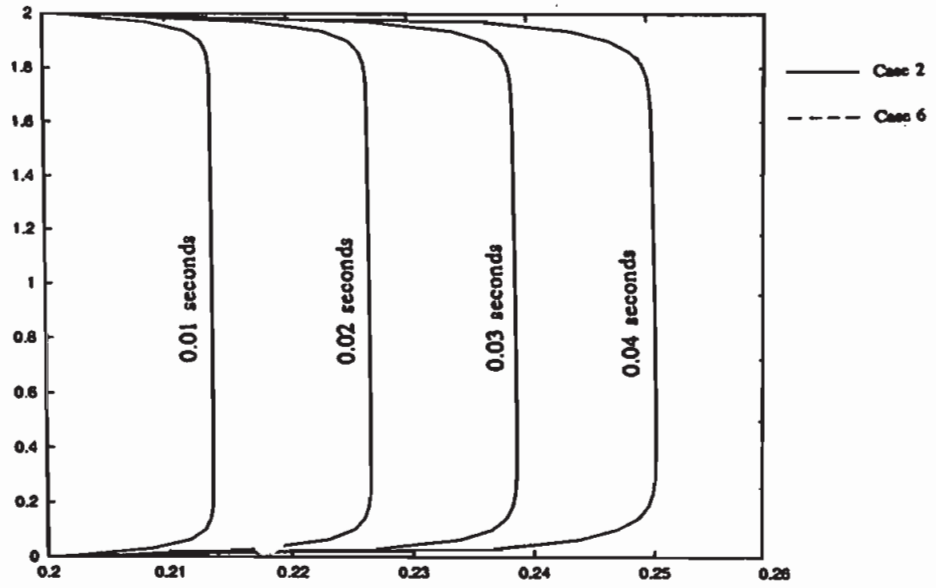

(*b*)

Figure 7. Comparisons of temporal free surface distributions for (*a*) cases 1 and 5 and (*b*) cases 2 and 6.

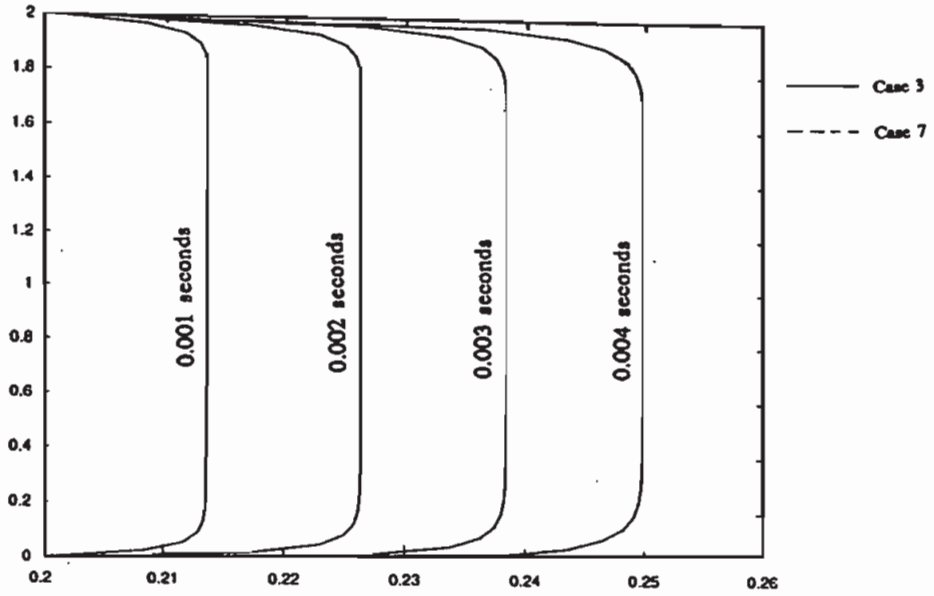

(*c*)

Figure 7. Comparisons of temporal free surface distributions for (*Continued*): (*c*) cases 3 and 7.

increased to 0.18 for case 7, the difference in the temporal free surface distribution becomes even more insignificant, as shown in Figure 7*c*. As can be seen in Figure 8*c*, identical pressure distributions are obtained at 0.004 s. This shows that the capillary pressure does not have a significant effect on the overall pressure distribution. Therefore, if the surface tension effect is accounted for in case 7, no difference will be encountered in the temporal free surface distribution and pressure distribution because the capillary pressure is insignificant in comparison with the applied pressure difference. It can be seen that for a higher Re, the surface tension will have a lesser impact on the free surface transport.

Figure 9 presents the temporal axial Nusselt number distributions for cases 5, 6, and 7 at selected times. Referring to Figure 9*a*, the temporal axial Nusselt number distributions at 0.4 s for case 5 are very similar to those of case 1 at 0.4 s, with minor differences for the region near the free surface. By examining axial Nusselt number distributions at 0.4 s depicted in Figure 9*a*, it can be seen that the effect of surface tension is not significant. For case 6 (Figure 9*b*), the difference becomes more insignificant, and for case 7 the difference becomes negligible. It can be concluded that the surface tension effect does not impact the temperature field as much as it affects the velocity and pressure fields.

Figures 10*a* and 10*b* depict comparisons of the temporal free surface distributions for case 8 and case 9 with and without surface tension effect. The Reynolds number for both cases is 0.57, which is higher than in case 3. On the basis of the conclusion drawn earlier, identical temporal free surface distribution and pressure

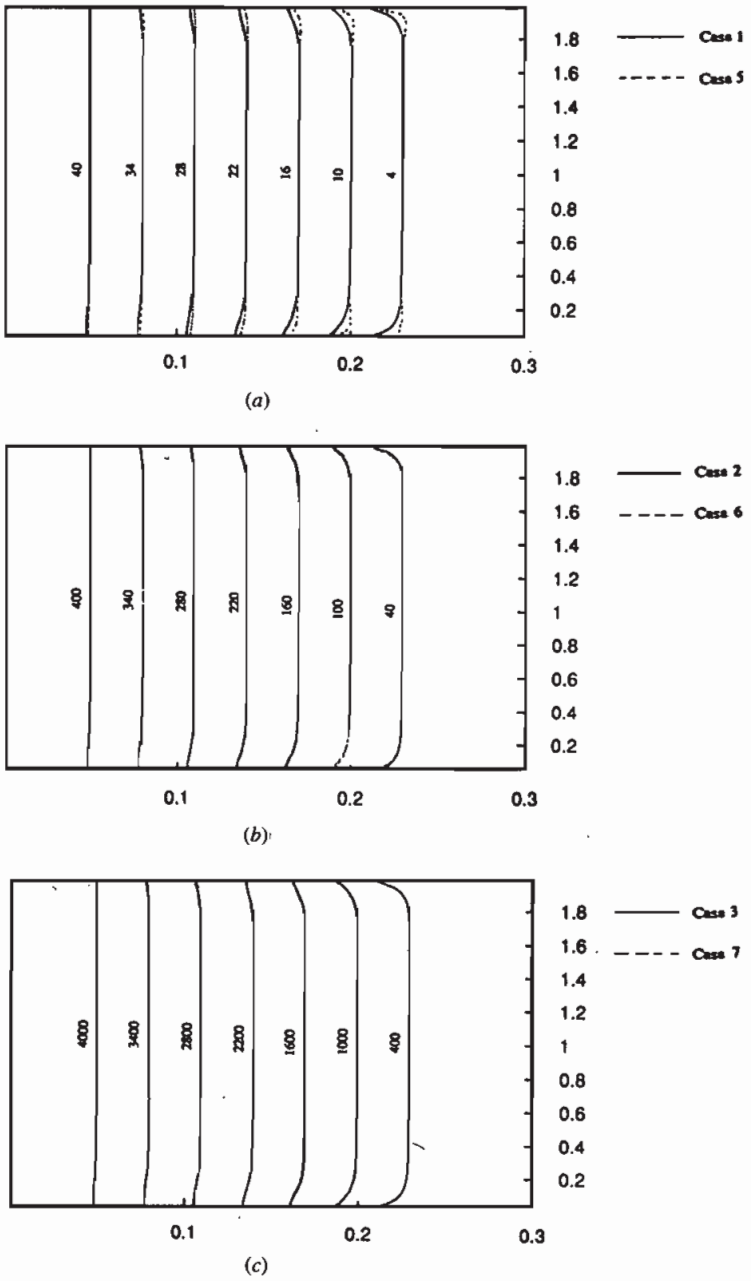

Figure 8. Temporal surface pressure distributions for (*a*) cases 1 and 5 at 0.4 s, (*b*) cases 2 and 6 at 0.04 s, and (*c*) cases 3 and 7 at 0.004 s.

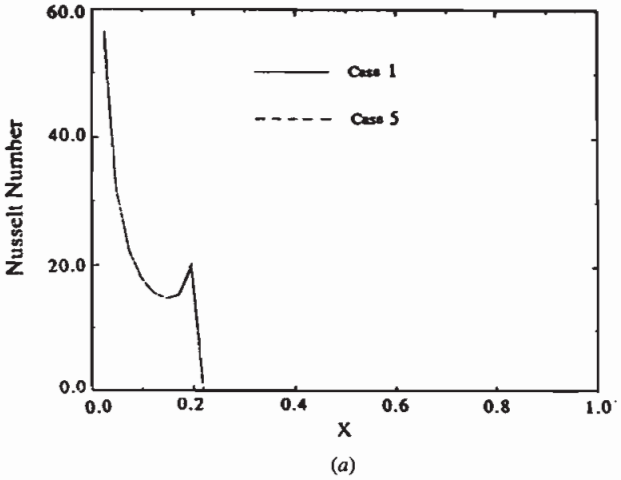

(*a*)

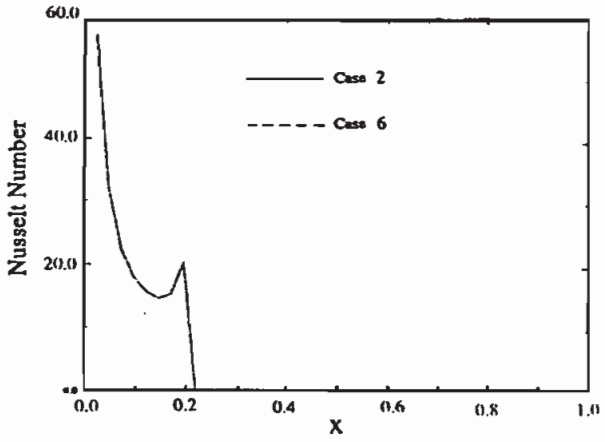

(*b*)

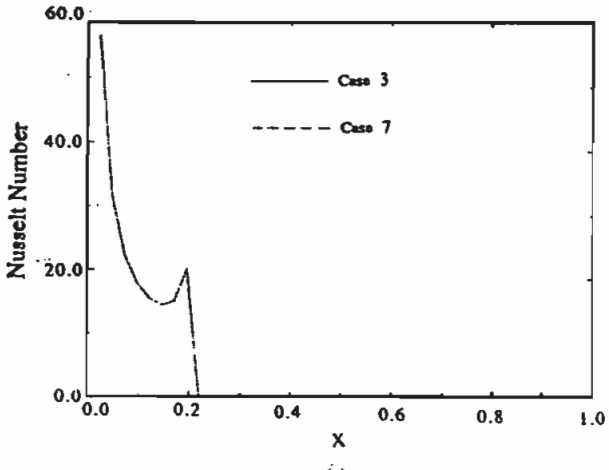

(*c*)

Figure 9. Comparison of axial Nusselt distribution for (*a*) cases 1 and 5 at 0.4 s, (*b*) cases 2 and 6 at 0.04 s, and (*c*) cases 3 and 7a at 0.004 s.

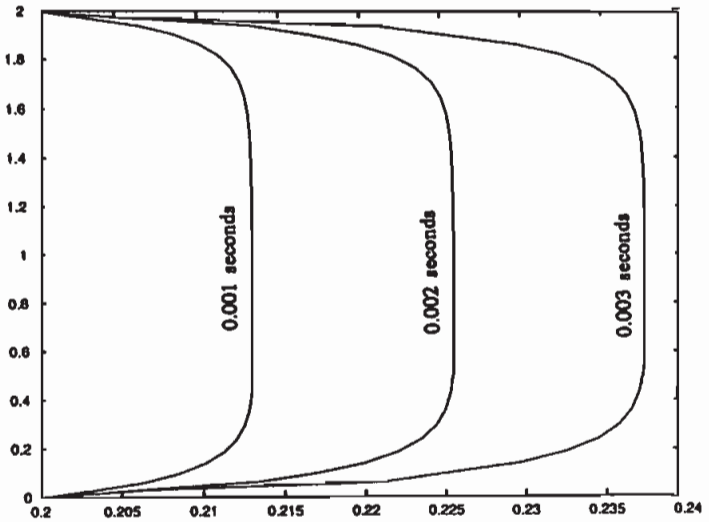

(*a*)

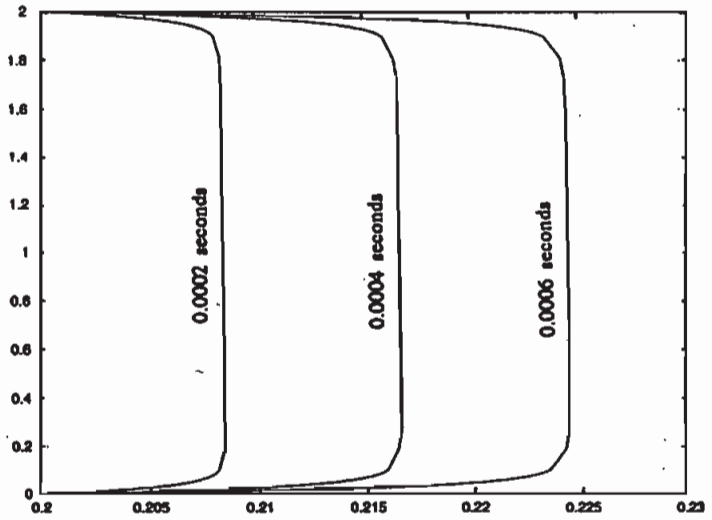

(*b*)

Figure 10. Comparisons of temporal free surface distributions with and without surface tension effect for (*a*) case 8 and (*b*) case 9.

and temperature fields are to be expected. It is therefore confirmed that, for $Re_K > 1$, the surface tension effect has a negligible impact on the free surface momentum and energy transports.

CONCLUSIONS

A phenomenological analysis of free surface transport through porous media is presented. The present work constitutes one of the first investigations of free

surface momentum and energy transport through porous media, as well as the first application of the marker-and-cell method to investigate the free surface transport phenomena in porous media using the Brinkman–Forchheimer–extended Darcy model. Excellent agreements are observed when limiting cases of the present results are compared with existing analytical results. It is observed that an unsaturated zone is formed near the channel wall owing to the no-slip boundary condition. It is also observed that the size of the unsaturated area decreases as the filling process progresses owing to the vertical flow field resulting from a vertical pressure gradient. It is found that the surface tension effect on the free surface momentum transport is significant only for low Re_K flows.

The application of the no-slip condition results in the unsaturated zone, which retards the heat transfer through the channel wall. The dominance of the diffusive heat transfer for lower values of Re is demonstrated. It is found that the surface tension effect has less impact on energy transport than momentum transport and the surface tension effects altogether become insignificant for $\mathrm{Re}_K > 1$. It is also found that the boundary and inertial effects have a significant influence on the free surface transport through porous media. The current work constitutes a rigorous investigation of free surface momentum and energy transport through porous media, covering such applications as the injection molding process and the two-phase flow system. It also forms a foundation for further understanding of flow and heat transfer characteristics of free surface transport through porous media.

REFERENCES

1. M. Muskat, *The Flow of Homogeneous Fluids Through Porous Media*, 1st ed., Edwards, Ann Arbor, Mich., 1937.
2. V. Srinivasan and K. Vafai, Analysis of Linear Encroachment in Two-Immiscible Fluid Systems in a Porous Medium, *J. Fluids Eng.*, vol. 116, pp. 135–139, 1994.
3. S. C. Chen and K. Vafai, Analysis of Free Surface Momentum and Energy Transport in Porous Media, *Numer. Heat Transfer Part A*, vol. 29, pp. 281–296, 1996.
4. W. B. Young, K. Rupel, K. Han, L. J. Lee, and M. J. Liou, Analysis of Resin Injection Molding in Molds with Preplaced Fiber Mats, II: Numerical Simulation and Experiments of Mold Filling, *Polymer Composites*, vol. 12, pp. 30–38, 1991.
5. M. V. Bruschke and S. G. Advani, A Finite Element/Control Volume Approach to Mold Filling in Anisotropic Porous Media, *Polymer Composites*, vol. 11, pp. 398–405, 1990.
6. R. Lin, L. J. Lee, and M. Liou, Nonisothermal Mold Filling and Curing Simulation in Thin Cavities with Preplaced Fiber Mats, *Int. Polymer Proc.*, vol. VI, pp. 356–369, 1991.
7. K. Vafai and S. C. Chen, Analysis of Free Surface Transport Within a Hollow Glass Ampule, *Numer. Heat Transfer Part A*, vol. 22, pp. 21–49, 1992.
8. F. H. Harlow and J. E. Welch, Numerical Calculation of Time-Dependent, Viscous, Incompressible Flow of Fluid with Free Surface, *Phys. Fluids*, vol. 8, pp. 2182–2189, 1965.
9. B. J. Daly and W. E. Pracht, Numerical Study of Density-Current Surge, *Phys. Fluids*, vol. 11, pp. 15–30, 1968.
10. C. W. Hirt and J. P. Shannon, Free-Surface Stress Condition Incompressible-Flow Calculations, *J. Comput. Phys.*, vol. 2, pp. 403–411, 1968.
11. R. K.-C. Chan and R. L. Street, A Computer Study of Finite Amplitude Water Waves, *J. Comput. Phys.*, vol. 6, pp. 68–94, 1970.

12. C. W. Hirt, J. L. Cook, and T. D. Butler, A Lagrangian Method for Calculating the Dynamics of an Incompressible Fluid with Free Surface, *J. Comput. Phys.*, vol. 5, pp. 103–124, 1970.
13. C. S. Frederiksen and A. M. Watts, Finite-Element Method for Time-Dependent Incompressible Free Surface Flow, *J. Comput. Phys.*, vol. 39, pp. 282–304, 1981.
14. S. C. Chen and K. Vafai, An Experimental Investigation of Free Surface Transport, Bifurcation and Adhesion Phenomena as Related to a Hollow Glass Ampule and a Metallic Conductor, *J. Heat Transfer*, vol. 114, pp. 743–751, 1992.
15. K. Vafai and C. L. Tien, Boundary and Inertia Effects on Flow and Heat Transfer in Porous Medium, *Int. J. Heat Mass Transfer*, vol. 24, pp. 195–203, 1981.
16. K. Vafai and C. L. Tien, Boundary and Inertial Effects on Convective Mass Transfer in Porous Media, *Int. J. Heat Mass Transfer*, vol. 25, pp. 1183–1190, 1982.
17. A. Amiri and K. Vafai, Effects of Boundary Conditions on Non-Darcian Heat Transfer Through Porous Media and Experimental Comparisons, *J. Numer. Heat Transfer Part A*, vol. 27, pp. 651–664, 1995.
18. J. C. Koh, J. C. Dutton, B. A. Benson, and A. Fortini, Friction Factor for Isothermal and Nonisothermal Flow Through Fibrous Porous Media, *J. Heat Transfer*, vol. 99C, pp. 367–373, 1977.
19. K. Vafai, Convective Flow and Heat Transfer in Variable-Porosity Media, *J. Fluid Mech.*, vol. 147, pp. 233–259, 1984.
20. K. Vafai and S. J. Kim, Forced Convection in a Channel Filled with a Porous Medium: An Exact Solution, *J. Heat Transfer*, vol. 111, pp. 1103–1106, 1989.